IEEE Access
Multidisciplinary | Rapid Review | Open Access Journal

Received October 18, 2018, accepted November 24, 2018, date of publication December 3, 2018,
date of current version December 27, 2018.

Digital Object Identifier 10.1109/ACCESS.2018.2884451

Design and Control of a Wearable Hand Rehabilitation Robot

LONG CHENG[1,2], (Senior Member, IEEE), MIAO CHEN[1], AND ZHENGWEI LI[1]

[1]State Key Laboratory of Management and Control for Complex Systems, Institute of Automation, Chinese Academy of Sciences, Beijing 100190, China
[2]School of Artificial Intelligence, University of Chinese Academy of Sciences, Beijing 100049, China

Corresponding author: Long Cheng (long.cheng@ia.ac.cn)

This work was supported in part by the National Nature Science Foundation under Grant 61873268, Grant 61421004, and Grant 61633016, in part by the Research Fund for Young Top-Notch Talent of National Ten Thousand Talent Program, in part by the Beijing Municipal Natural Science Foundation under Grant 4162066, and in part by the Major Science and Technology Fund of Beijing under Grant Z181100003118006.

ABSTRACT This paper proposes a wearable hand rehabilitation robot for assisting patients to do rehabilitation training such as the flexion and extension of fingers. This robot prototype has a modularized structure with nine degrees of freedom for the independent control of the patient's fingers. To alleviate the weight applied on the patient's hand and arm, the entire control system is placed in the patient's backpack and the cable-driven approach is employed to achieve the long-distance power transmission. Because of the repetitive training manner and the existence of external disturbances, a controller combining the iterative learning control (ILC) and the active disturbance rejection control (ADRC) has been proposed for the control of the finger's joints. The contributions of this paper lie in the robot's modularized structure design and the proposed "ILC + ADRC" controller. Experimental results have verified the function of the proposed robot and demonstrated the satisfactory control performance achieved by the proposed controller.

INDEX TERMS Hand rehabilitation, exoskeleton, cable-driven, modularized structure, active disturbance rejection controller (ADRC), iterative learning control (ILC).

I. INTRODUCTION

In recent years, there is a huge population of stroke patients around the world (e.g., approximately 700,000 people experience a new or recurrent stroke each year in US [1]). Stroke often results in a combination of cognitive, sensory and motor impairments [2]. About two thirds of stroke survivors suffer from partial paralysis at the level of arm and hand [3]. Due to its important role in daily life, regaining the hand function is identified as one urgent demand of people with paralyzed limbs [4]. It is reported that intensive practice of repetitive movements can help improve the limb's strength and functional recovery [5]. However, the traditional treatment is a long-term process requiring a large number of medical and human resources, which cannot be fully satisfied by the limited number of rehabilitation therapists.

Fortunately, various rehabilitation/assistant robots have been developed in these years and have been clinically proved to be effective [6]. In particular, a series of studies have been carried out for the analysis of hand rehabilitation robots [7], [8]. Among hand rehabilitation robots, the exoskeleton is popular and welcomed because it is designed based on the specific human body and can provide data of every anatomical joint to the therapist. There are two ways to categorize the exoskeleton hand rehabilitation robots:

- From the design aspect, it includes the robot based on the fixed-frame platform [9], [10] and the portable robots [11]–[13]. Robots based on the fixed-frame platform have many advantages, such as precision and load reduction for patients. However, these robots are extremely heavy and have a negative effect on the arm training (studies have shown that simultaneous training of the arm and fingers can improve the rehabilitation performance [14]). The portable robot can overcome these limitations effectively [15]. However, the hardware control systems of these robots are often placed on the patient's arm, which increases the load on the arm and usually leads to the loss of dexterity and the limited arm's reachable workspace [16].
- From the actuation aspect, hand rehabilitation exoskeletons can be divided into three classes: the pneumatic-/hydraulic-driven robots [17]–[20], the motor-driven rigid-linkage robots [21]–[23] and the cable-driven robots [24]–[27]. Pneumatic-/hydraulic-driven robots are usually soft robotic gloves which are inherently

compliant and lightweight, however, they are hard to be controlled and the volumes of their control systems are relatively large. The motor-driven rigid-linkage exoskeleton can calculate the finger's motion easily through the motor's movement and provide the bi-directional interaction force. However, the applied force may be dissipated by the intermediate linkages. Furthermore, rehabilitation robots based on the intermediate linkage are likely to cause the second hurt of patients [28]. Cable-driven robots are more compliant than the motor-driven rigid-linkage exoskeleton and have a relatively small volume. This type of robots can achieve the long-distance power transmission because of the bendable and soft properties of cables.

By summarizing the above discussions, a useful robot should satisfy the following basic requirements: (1) be safe and can avoid the secondary injury of patients; (2) be able to effectively assist patients to do rehabilitation training; and (3) do not bring the patients extra burden and inconvenience in the assistance. These observations give the motivation of designing a new hand rehabilitation robot in this study.

The proposed design of the hand rehabilitation robot is a portable exoskeleton with nine degrees of freedom that can assist patients to do the finger's flexion and extension. This robot is: (1) portable: it does not need a fixed support and can be conveniently worn by users to do rehabilitation training; (2) lightweight: the entire control system is placed in a backpack or amounted on the wheelchair for patients with limited mobility. This dramatically reduces the extra weight on the patient's arm and hand; (3) cable-driven: the remote control is achieved by the cable-driven approach which also adds compliance for the human-robot interaction; (4) safe: there are physical limits in the exoskeleton's joints. A programming/software limit is also added to guarantee the bending angle within a safe range. Finally, this robot's design has a distinguished feature: modularized structure. The joint section of the exoskeleton is designed as a shell-like one according to the bionics design principle. Each finger exoskeleton is composed of several standard ''shells'' and ''connecting rods'', which makes it convenient to be disassembled, assembled and maintained.

In clinical practices, therapists usually assist patients to do repetitive finger movements. When assisted by robots, the robot must be able to control the finger's flexion or extension to a specified angle according to the therapist's instruction. There have already been some studies regarding the control strategy applied to the hand rehabilitation robot. Park *et al.* utilized the proportional, integral and differential (PID) control for the finger's position control [29]. Chiri *et al.* [25] used the PID controller to track the finger's reference trajectory. Wu *et al.* [30] proposed a variable integral PID controller for the finger's trajectory tracking as well. Jones *et al.* [31] developed a PI controller along with an auxiliary torque compensation for the finger's position and torque control. Polygerinos *et al.* [18] presented a sliding-mode controller (SMC) for the finger's flexion and extension.

The above review shows that most controllers of hand exoskeletons employ the basic PID idea. However, the parameter setting of the PID controller is complicated and is very dependent on experiences. And the PID controller has a limited performance on the disturbance rejection. Few attempts on the advanced controllers such as SMC require the accurate mathematical model of robots. In this paper, the active disturbance rejection controller (ADRC) is employed for fulfillment of the finger's movement control because of its favourable ability of disturbance rejection. The ADRC approach inherits the advantages of classical PID control, and does not depend on the robot's dynamic model either. Furthermore, it can be easily observed in the therapist-assisted rehabilitation training that the finger's movement trajectory is repetitive. In the control community, the iterative learning control (ILC) method is known to be effective for uncertain dynamical systems that operate repetitively. Through error iterations, both the steady-state performance and the transient response can be improved. It is noted that the ILC approach has been applied to the rehabilitation robot. In [32], a novel robust iterative learning control, the normalized iterative feedback tuning technique, is applied to the training of a compliant parallel ankle rehabilitation robot. In [33], an online iterative learning linear quadratic regulator is proposed for the trajectory tracking control of a leg rehabilitation exoskeleton. In [34], the ILC with the input-output linearization technique has been used to generate the functional electrical stimulation for the upper limb reference tracking. In [35], the ILC is employed not only for the tracking control of one upper limb rehabilitation robot but also for updating the tracking reference. In [36], the ILC is used for the compliant and safe interaction between the rehabilitation robot and the patient. In these practices, the ILC approach has received a great success. However, to the best of the authors' knowledge, the ILC approach has not been used in the hand rehabilitation robot, which motivates us to use the ILC approach when designing the controller for the hand rehabilitation robot. This paper proposes a novel controller, the ''ILC+ADRC'' controller, for the finger's position and tracking control. By using the ILC as a feedforward compensation term to shape the transient control performance and using the ADRC as a feedback term to attenuate external disturbances, the proposed composite controller is expected to have a satisfactory control performance which has been demonstrated by experiments conducted in this paper.

The rest of this paper is organized as follows. Section II introduces the system design of this hand rehabilitation exoskeleton. The workspace of this robot is analyzed in Section III. Section IV introduces the ''ILC+ADRC'' control algorithm. Section V provides the experimental results and related analysis. Finally, Section VI concludes the study and presents suggestions for future work.

II. DESIGN OF HAND REHABILITATION ROBOT

The proposed hand rehabilitation robot includes three parts: the remote driving backpack, the power transmission and the

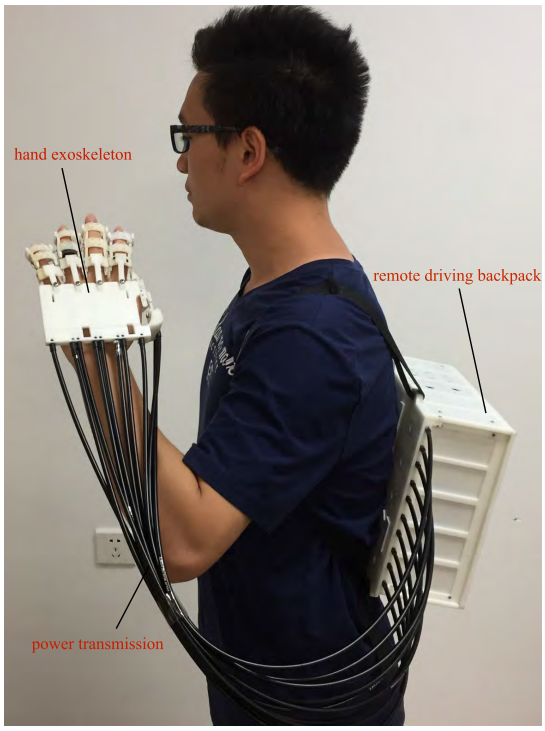

FIGURE 1. Proposed hand rehabilitation robot including the remote driving backpack, the power transmission and the hand exoskeleton.

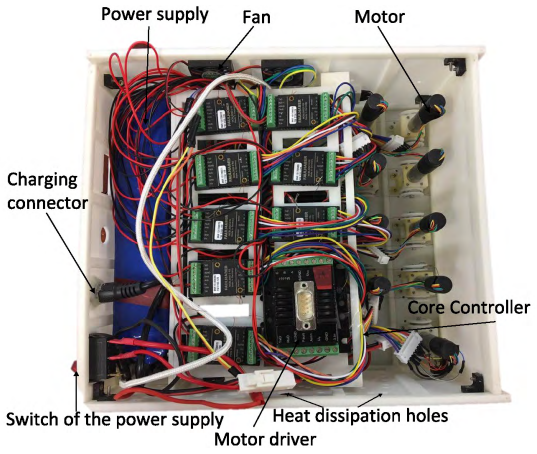

FIGURE 2. Remote driving package system including motors, motor drivers, controller, and power supply modules.

hand exoskeleton (see Fig. 1). The following three subsections introduce the design details.

A. REMOTE DRIVING BACKPACK

The entire robot driving system including the motor, driver, controller, and power supply modules is placed in one backpack whose size is: 275 × 230 × 110mm. The details of the backpack are shown in Fig. 2.

The motor module including nine motors and nine motor gearboxes is designed to generate the driving force for the hand exoskeleton. Here the robotic thumb is driven by one motor and other fingers are driven by two motors. The motor

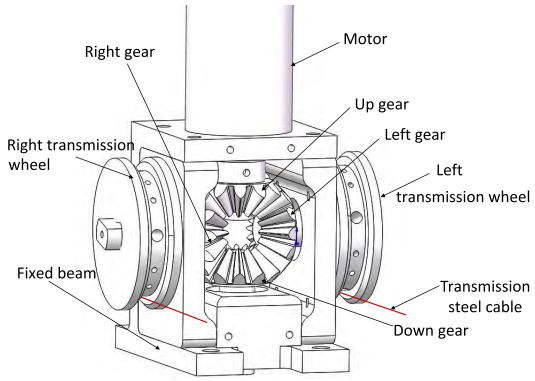

FIGURE 3. Design of the motor's gearbox.

used in this paper is a DC brushless servo motor manufactured by Faulhaber (1226A012B K1855, Faulhaber, Germany). In order to maximize the motor's usage, one motor is used to achieve both the flexion and the extension of the driving joint. To this end, the motor gearbox has two steel-cable transmission wheels on its both sides (see Fig. 3). The left transmission wheel has the same rotation direction as the left gear. Likewise, the right transmission wheel rotates in the same direction as the right gear. The movement of the upper gear is consistent with the motor. Since the left gear and the right gear are engaged to the upper gear, the rotation directions of the left transmission wheel and the right transmission wheel are opposite when the motor rotates. Because the winding directions of two transmission cables are the same, either the left transmission cable or the right transmission cable is in the stretched state. This leads to the fact that the motor's forward rotation causes the driving joint's extension and the backward rotation causes the driving joint's flexion. The motor driver (MCBL 3002S, Faulhaber, Germany) is compatible with the selected motor. The motor driver is connected with the controller through the controller's communication serial port. The core controller is the DA-1000 Processor Affordable Fanless Embedded Computer which has two RS-232/422/485 communication ports. Controller and motor drivers are powered by a 14V, 10000mAh Li-ion battery which is capable of working at least 5 hours in the highest usage case. The charging connector and the switch of the power supply are embedded in the rear panel of the backpack for easy charging and power control. Both small holes on the surface of the backpack and two fans are used for the heat dissipation.

B. POWER TRANSMISSION

The cable-driven power transmission approach is used to transmit the driving force generated by the motor to the hand exoskeleton. The steel cable with a diameter of 0.265mm, which can bear a force of 95N, is selected as the transmission cable due to its high strength, stable, reliable and corrosion resistance characteristics. One end of the steel cable is fixed at the transmission wheel and the other end is connected to the hand exoskeleton. In order to constrain the path of the

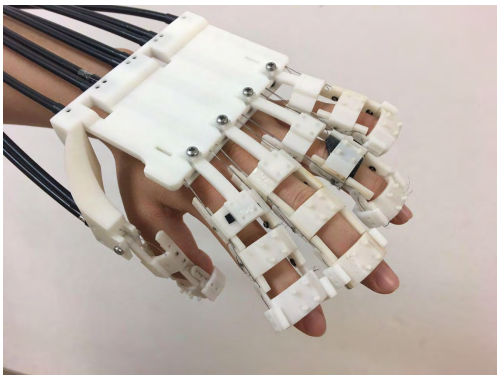

FIGURE 4. One subject wearing the hand exoskeleton.

transmission steel cable, a steel cable housing (black tube in Fig. 1) is used. The diameter of the steel cable housing is 4.9mm. In order to reduce the power loss caused by the friction between steel cables, one steel cable housing contains only two steel cables. The steel cable housing includes three layers: pipe jacket, helical inner tube and PVC lubrication layer. The helical inner tube is a metal pipe that formed by helical steel, which ensures that the wire tube does not have a transverse tensile deformation. The PVC lubrication layer can reduce the friction between the steel cable housing and the steel cable.

C. HAND EXOSKELETON

The hand exoskeleton directly interacts with the patient's hand (see Fig. 4). This hand exoskeleton's weight is 206g, which is a relatively small burden for patients. The hand exoskeleton includes the palm fixation mechanism and the finger exoskeleton mechanism. The role of the palm fixation mechanism is to fix the finger exoskeleton mechanism at a desired position. Finger exoskeleton mechanism is the executive body, which is used to assist patients to do finger's flexion and extension.

1) PALM FIXATION MECHANISM

The palm fixation mechanism contains five fixed positions for finger exoskeleton mechanisms. The fixed position of the thumb is the function position of the thumb. Fixed positions of the index finger, middle finger, ring finger and little finger are evenly distributed in the front of the palm fixation mechanism. The ''arc'' design ensures that the space between two fingers is adjustable to adapt to different patients' hands. At each fixed position, there are two holes of a diameter of 0.85mm, which are used as the passing passage of the steel cable. Ten holes of the diameter of 5.8mm are made at rear of the palm fixation mechanism for fixing the steel cable housing.

2) FINGER EXOSKELETON MECHANISM

The middle finger exoskeleton is taken as an example for introduction, whose structure is shown in Fig. 5(a). For each patient's finger ''linkage'', there is a corresponding shell-like

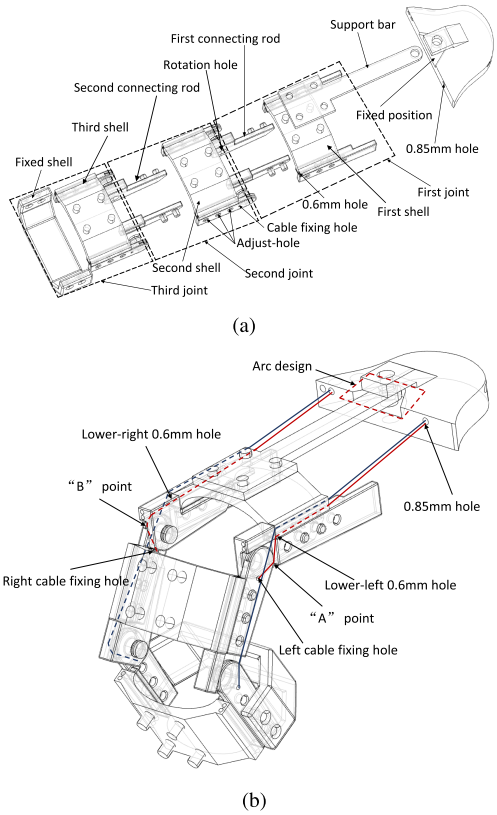

FIGURE 5. The middle finger exoskeleton structure. (a) The outlook of the middle finger exoskeleton before flexion. (b) The outlook of the middle finger exoskeleton after flexion.

mechanism (we call it ''shell''. See the first shell in Fig. 5(a) for example). On both sides of the shell, there are two holes of a diameter of 0.6mm which are used as the passing path of the steel cable. All the shells are manufactured to be identical. This is consistent with the modularized design idea. As a basic component, shells can be exchangeably used. If one shell is broken, it can be easily replaced by other shells and we do not need to amend the entire finger exoskeleton. The top of the first shell is connected to the palm fixation mechanism by the support bar at the middle finger exoskeleton's fixed position. The bottom of the first shell is connected to the first connecting rod at two ''adjust-holes'' of the first shell. By choosing different ''adjust-holes'', the length of the robotic finger ''linkage'' can be adapted to different finger sizes. The connection between the first shell and the first connecting rod is ''rigid'' (i.e., no relative motion). Therefore, we call the first shell and the first connecting rod together as the first joint. The second shell is connected to the first connecting rod through the second shell's rotation hole. When the second shell moves downward around its rotation hole, the angle between the first joint and the second shell changes and therefore the finger ''linkage'' wearing the second shell bends. It is noted that there is a physical limit in the connecting rod for the safety reason. This physical limit makes sure that the angle between the first joint and the second shell never exceeds the predesigned limit. The second shell

together with the second connecting rod form the second joint. The top of the third shell is connected to the second connecting rod through its rotation hole while the bottom of the third shell is connected to the fixed shell which is designed for fixing the finger's tip. The third shell together with the fixed shell form the third joint.

The path of the transmission steel cable is shown in Fig. 5(b) (see the solid and dash lines). It should be noted that the path of the left transmission cable is different with the one of the right transmission cable. Let us take the second shell for example. The left transmission cable goes through the ''lower-left 0.6mm hole'' of the first shell to the ''left cable fixing hole'' of the second shell via the ''A'' point. The right transmission cable goes through the ''lower-right 0.6mm hole'' of the first shell to the ''right cable fixing hole'' of the second shell via the ''B'' point. In the view of the entire system, the path of the transmission cable starts from the transmission wheel in the motor driver system, then goes through the 0.85mm hole located in the front of the backpack. After that, the cable moves inside the cable housing to the 0.85mm hole located in the palm fixation mechanism. Finally, it reaches the finger exoskeleton and is fixed at the ''left/right cable fixing hole'' of the second shell. When the left transmission cable is actively pulled backward by the left transmission wheel, the shell moves downward around its rotation hole, resulting in the flexion of the corresponding finger ''linkage''. At the same time, the right transmission cable is passively pulled forward by the shell. Since the rotation directions of the left transmission wheel and the right transmission wheel are opposite, the right transmission cable still keeps in the stretched state. Likewise, when the right transmission cable is actively pulled backward by the right transmission wheel, the shell moves upward around its rotation hole, resulting in extension of the corresponding finger ''linkage''. And the left transmission cable is passively pulled forward by the shell and is kept in the stretched state due to the rotation of the left transmission wheel. If the path of the right transmission cable is the same as the one of the left transmission cable, no matter which cable is actively pulled, the shell always moves downward around its rotation hole since the transmission cable can only supply the pulling force. This leads to the fact that only the flexion state can be achieved, which cannot be accepted.

Remark 1: Compared to some wearable hand rehabilitation robots, the proposed robot prototype has several features. For example, compared to the designs of soft-body robots in [17]–[20], the proposed robot can achieve the relatively precious control of the robot's joint. Compared to the motor-driven rigid-linkage robot designs [21]–[23], extra weights on the patients can be reduced by the proposed design. For the cable-driven robot designs, in [24], the rotation axes of the exoskeleton are not well aligned with the human's finger joints; compared to [25], the proposed exoskeleton only uses one motor to achieve both the flexion and the extension of one joint; in [26], the driving cables unwinds from the motors easily when the robot is not worn; compared to [27], the proposed robot could control the extension/flexion of both the proximal interphalangeal (PIP) joint and the distal interphalangeal (DIP) joint, respectively. In addition, the proposed exoskeleton has the modularized structure (the shell-like mechanism) which can be assembled and maintained easily.

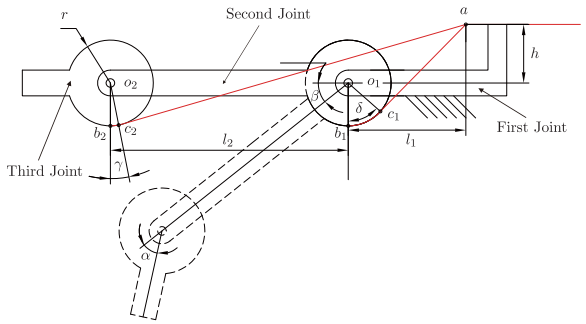

FIGURE 6. Simplified model of the finger exoskeleton mechanism.

III. WORKSPACE ANALYSIS

Compliance with the patient's hand anatomy is one premise for the hand rehabilitation robot. And the robot should not constrain the finger's movement space. Therefore, it is necessary to analyze the robot's workspace. For the sake of simplicity, the finger exoskeleton mechanism is simplified as the one shown in Fig. 6.

The second joint can rotate around o_1 through the cable b_1c_1a, and the third joint rotates around o_2 by the cable b_2c_2a. The horizon distance from o_1 to ''a'' point is denoted by l_1, and the distance between o_1 and o_2 is denoted by l_2. The cable b_1c_1a is tangent to the second joint at c_1, and the cable b_2c_2a is tangent to the third joint at c_2. When all joints are in horizontal position, the starting points (b_1, b_2) of two cables are located just below the joint's centers (o_1, o_2), respectively. The angle between the second joint and the horizontal plane is β, and the angle between the third joint and the second joint is α. It is set that $\angle b_1o_1c_1 = \delta$ and $\angle b_2o_2c_2 = \gamma$.

When $\beta < \delta$, the relationship between the moving distance L_1 of cable b_1c_1a and the second joint's angle β can be expressed as below:

$$L_1 = \frac{\beta \cdot \pi r}{180}. \tag{1}$$

When $\beta > \delta$, this relationship can be expressed by the following formula:

$$L_1 = \sqrt{(h + r\cos\delta)^2 + (l_1 - r\sin\delta)^2} - \sqrt{(h + r\cos\beta)^2 + (l_1 - r\sin\beta)^2} + \frac{\delta \cdot \pi r}{180}. \tag{2}$$

The relationship between the moving distance L_2 of cable b_2c_2a and α and β is more complicated. It can be divided into two cases:

- when $\alpha < 90^\circ + \angle ao_2o_1 - \angle ao_2c_2$, then

$$\alpha < 90^\circ - \cos^{-1}\left(\frac{r}{\sqrt{(l_2\cos\beta + l_1)^2 + (l_2\sin\beta + h)^2}}\right) + \cos^{-1} \times \left(\frac{(l_2\cos\beta + l_1)^2 + (l_2\sin\beta + h)^2 + l_2^2 - l_1^2 - h^2}{2l_2\sqrt{(l_2\cos\beta + l_1)^2 + (l_2\sin\beta + h)^2}}\right). \quad (3)$$

  In this case, the relationship between the moving distance L_2 of cable b_2c_2a and α and β can be expressed as below:

$$L_2 = \frac{(\alpha + \beta)\cdot \pi r}{180} - \sqrt{(l_1 + l_2)^2 + h^2 - r^2} + \sqrt{(l_1 + l_2\cos\beta)^2 + (h + l_2\sin\beta)^2 - r^2}. \quad (4)$$

- when $\alpha > 90^\circ + \angle ao_2o_1 - \angle ao_2c_2$, then

$$\alpha > 90^\circ - \cos^{-1}\left(\frac{r}{\sqrt{(l_2\cos\beta + l_1)^2 + (l_2\sin\beta + h)^2}}\right) + \cos^{-1} \times \left(\frac{(l_2\cos\beta + l_1)^2 + (l_2\sin\beta + h)^2 + l_2^2 - l_1^2 - h^2}{2l_2\sqrt{(l_2\cos\beta + l_1)^2 + (l_2\sin\beta + h)^2}}\right). \quad (5)$$

  In this case, the relationship between the moving distance L_2 of cable b_2c_2a and the third joint angle α can be expressed by (6), shown at the bottom of the next page.

By the above analysis, the finger's workspace can be calculated. When points o_1, b_1 and a are in the same line, the second joint moves to its limit position β_{max} which is expressed by

$$\beta_{max} = \delta + \arctan\frac{\sqrt{(h + r\cos\delta)^2 + (l_1 - r\sin\delta)^2}}{r}. \quad (7)$$

When points o_2, b_2 and a are in the same line, the third joint moves to its limit position α_{max} which is expressed by

$$\alpha_{max} = 90^\circ - \beta + \arctan\frac{l_2\sin\beta + h}{l_2\cos\beta + l_1}. \quad (8)$$

Then the workspace of the finger exoskeleton can be shown in Fig. 7. According to the above two equations, the limit position of the PIP joint is 116.3° and that of the DIP joint is 124.4°. By the anthropometric data reported in [37], the proposed finger exoskeleton does not constrain the human finger's movement range.

IV. MEASUREMENT AND CONTROL SYSTEMS

A. MEASUREMENT SYSTEM

To design controllers for the rehabilitation training, it is necessary to measure the patient's finger angle. The proposed robot system is equipped with the curvature sensor

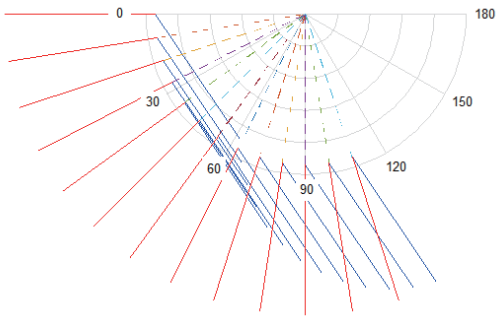

FIGURE 7. Plot of the workspace of the finger exoskeleton. (The dash line denotes the motion range of the PIP. The red solid line and the blue solid line together denote the movement range of the DIP when the PIP is at a specific position. It can be seen that the movement range of the PIP is from 0° to 116.3°; the maximum movement range of the DIP is from 0° to 124.4° when the PIP is at the initial position 0°).

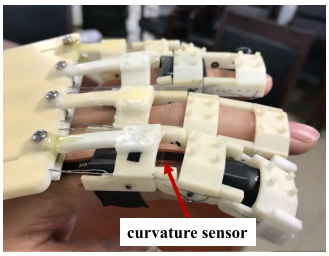

FIGURE 8. Placement of the curvature sensor.

(Flex 2.2, Spectrasymbol, USA) and the Hall sensor (K1855, Faulhaber, Germany). The curvature sensor is placed along the patient's finger, which can be seen in Fig. 8. The Hall sensor is amounted on the motor axis to detect the rotation angle of the motor. The safety rotation range of the motor can be determined by the pre-designed safety movement range of the finger exoskeleton by (1), (2), (4) and (6). When the value of the Hall sensor exceeds the motor's safety limit, the motor immediately stops to prevent the patient's secondary injury. The curvature sensor is used to detect the actual bending angle of the patient's finger. This sensor is calibrated by a commercial data glove (WISEGOLVE15, Xintian Vision Technology company, China) which can collect the finger's bending angle. The calibration process includes two steps: (1) the real finger's bending angle is measured by the commercial data glove; and (2) train a three-layer back-propagation (BP) neural network to find the relationship between the readout of the curvature sensor and the real finger's bending angle.

In the calibration experiment, a healthy volunteer is recruited to move his/her finger from the extension status to the flexion status and then go back to the extension status. A total of 380 experiment data are collected, which are divided into two parts: 85% of data are used as the training set and 15% of data are used as the testing set. The number of neurons in the hidden layer is 40. The hyperbolic tangent sigmoid function is chosen as the transfer functions of neurons in the hidden layer. The transfer functions of neurons in the input

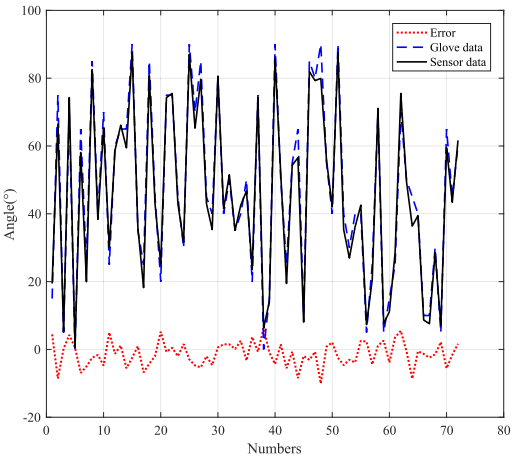

FIGURE 9. Calibration of the curvature sensor. The average of the absolute errors is 3.1°.

and output layers are the unit linear function. The calibration result is shown in Fig. 9. It can be seen that the maximum calibration error is 10.1° and the average of the absolute errors is 3.1°, which meets the experiment requirement.

B. CONTROL ALGORITHM

After obtaining the finger's bending angle, it is ready to design a closed-loop control algorithm. First of all, the core controller sets the finger's bending angle's movement trajectory $\theta_d(k)$. Then the curvature sensor at the finger exoskeleton collects the actual finger's bending angle and feeds it back to the core controller. After that, the core controller calculates the control effort by certain control algorithm and sends the control effort to the specific motor driver to control the motor's rotation. In this paper, the ADRC algorithm is selected as the desired control algorithm because it is not dependent on the robot's mathematical model and can use the expanded state observer to estimate and compensate the external disturbances in real time. According to [38], the ADRC algorithm can be described by the following equation

$$u(k) = \frac{k_p}{b}e(k) + \frac{k_p\omega}{b}\sum_{i=0}^{k} e(i) - \frac{\omega}{b}\theta(k), \quad k = 1, \cdots, N_K, \tag{9}$$

where N_K is the number of time sampling points, $u(k)$ is the control input (the motor's rotation angle); $\theta(k)$ is the current finger's bending angle; $e(k)$ is the difference between $\theta_d(k)$ and $\theta(k)$; k_p, b and w are parameters to be adjusted.

Furthermore, the rehabilitation training assisted by the therapist is usually repetitive. It means that the trajectory of the finger's bending angle is almost periodical, which is very suitable for the ILC strategy. Moreover, the ILC also requires little knowledge about the robot's dynamics. In this paper, the high-order ILC algorithm proposed in [39] is adopted as the feedforward controller of the finger exoskeleton. The high-order ILC algorithm requires an off-line training process. The controller updating algorithm can be described by the following equation

$$u_{j+1}(k) = u_j(k) + k_{p1}e_j(k+1) + k_{p2}e_{j-1}(k+1), \quad k = 1, \cdots, N_K, \quad j = 1, \cdots, N_J, \tag{10}$$

where k_{p1} and k_{p2} represent the proportional parameters of the j-th iteration and the $(j-1)$-th iteration, respectively; N_J is the total number of iterations. $u_j(k)$ is the control input for the j-th iteration; $e_j(k)$ is the difference between $\theta_d(k)$ and $\theta(k)$ during the j-th iteration. When the iteration of the controller updating algorithm defined by (10) terminates, the controller with the smallest tracking error among all iterations is selected as the final ILC feedforward controller and is denoted by $u_{ILC}(k)$. The off-line learning process of the high-order ILC controller is summarized in Algorithm 1.

Since the ILC algorithm can handle the repetitive motion control and the ADRC algorithm can deal with the disturbance, a better control performance can be expected if the advantages of both control algorithms are combined together. Therefore, this paper proposes a composite controller defined by (11) where the ILC algorithm is

Algorithm 1 High-Order ILC Control Algorithm

Initialization: $u_1(k) = 0, \theta_d(k), k = 1, \cdots, N_K$
for $j \leftarrow 1$ to N_J **do**
  for $k \leftarrow 1$ to N_K **do**
    Sending $u_j(k)$ to the motor driver
    Receive the respond of robot system
    Read the finger's bending angle and save it as $\theta_j(k+1)$
  end for
  for $k \leftarrow 1$ to N_K **do**
    if $j > 1$ **then**
      $e_{j-1}(k+1) \leftarrow \theta_d(k+1) - \theta_{j-1}(k+1)$
    else
      $e_{j-1}(k+1) \leftarrow 0$
    end if
    $e_j(k+1) \leftarrow \theta_d(k+1) - \theta_j(k+1)$
    $u_{j+1}(k) \leftarrow u_j(k) + k_1 e_j(k+1) + k_2 e_{j-1}(k+1)$
  end for
end for
Output: Select $u_{ILC}(k)$ with the best control performance from $u_1(k), \cdots, u_{N_J}(k)$.

$$L_2 = \frac{\gamma \cdot \pi r}{180} + \sqrt{(l_2\cos\beta + l_1)^2 + (l_2\sin\beta + h)^2 - r^2} - \sqrt{(l_2\cos\beta + l_1 - r\sin(\alpha+\beta))^2 + (l_2\sin\beta + h + r\cos(\alpha+\beta))^2}. \tag{6}$$

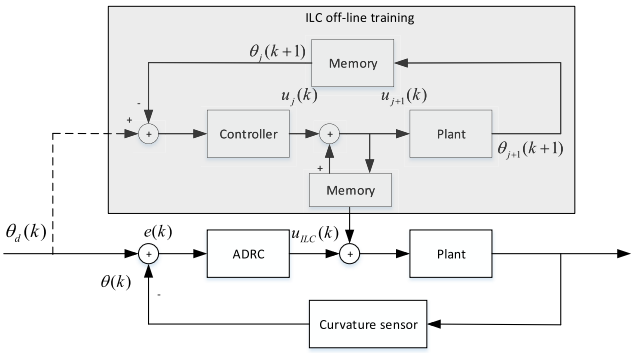

FIGURE 10. Block diagram of the entire control system.

selected as the feedforward control and the ADRC is set as a feedback control.

$$u(k) = u_{ILC}(k) + \frac{k_p}{b}e(k) + \frac{k_p\omega}{b}\sum_{i=0}^{k} e(i) - \frac{\omega}{b}\theta(k), \quad k = 1, \cdots, N_K. \tag{11}$$

The block diagram of the entire control system is shown in Fig. 10.

V. EXPERIMENTAL RESULTS AND DISCUSSIONS

A. FUNCTION VERIFICATION OF HAND REHABILITATION ROBOT

The overall appearance of the proposed hand rehabilitation robot has been shown in Fig. 1. In order to verify the function of the proposed rehabilitation robot prototype, an experiment has been conducted on a volunteer. In this experiment, the volunteer is required to complete the following finger training task: his/her fingers go from the complete flexion state to the complete extension state, then go back to the complete flexion state (this is called one training cycle). This training cycle is repeated three times. Figures 11(a)–11(f) show some intermediate snapshots of the hand in the training cycle.

In practice, patients are also required to fulfill some separation movements of fingers. These movements can be seen in the Fugl-Meyer scale for the motor function assessment. In the experiment, the hand rehabilitation robot is controlled to assist the volunteer to do three typical separation movements. Figures 11(g)-11(i) show some intermediate snapshots of the volunteer's fingers when conducting the separation movements.

From the experimental results, it can be seen that the volunteer can easily wear the hand exoskeleton and is not troubled by the weight of the hand exoskeleton; the hand exoskeleton can run in a stable and safe state in the training process. Therefore, this experiment verifies the function of the proposed hand rehabilitation robot.

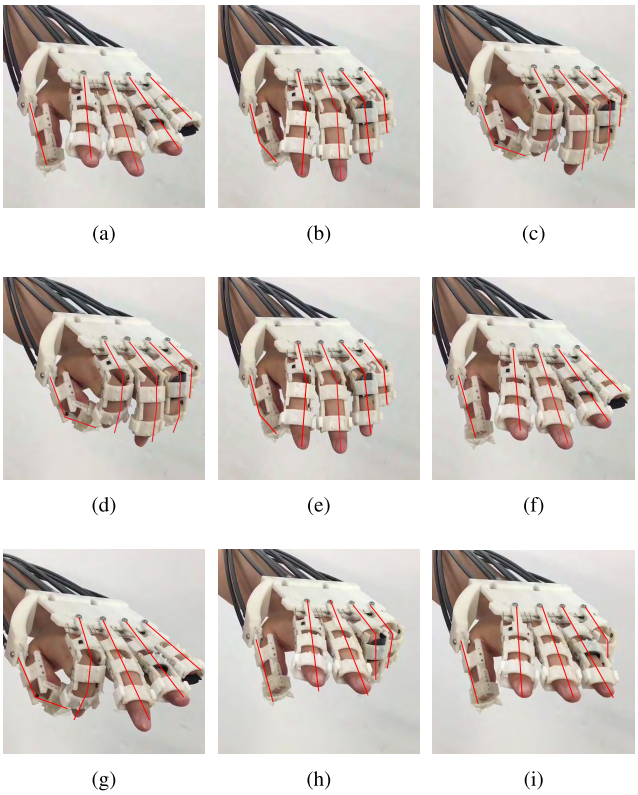

FIGURE 11. Some experiment snapshots of the volunteer assisted by the hand rehabilitation robot when conducting the finger's "flexion and extension" training and the separation movement training. (a) The initial state of flexion. (b) The intermediate state of flexion. (c) The final state of flexion. (d) The initial state of extension. (e) The intermediate state of extension. (f) The final state of extension. (g) Thumb and index finger flexion. (h) Ring finger and little finger flexion. (i) Little finger flexion.

B. VERIFICATION OF THE PROPOSED "ILC + ADRC" CONTROLLER

1) COMPARATIVE STUDY OF ADRC AND PID

As reported in Introduction Section, the most commonly used controller is the PID controller. In order to verify the performance of the proposed "ILC + ADRC" controller, a comparative experiment between the "ILC + ADRC" controller and the PID controller is necessary.

The first comparative experimental study is made to verify that whether only using the ADRC controller as the feedback controller can have a better performance than the traditional PID controller. Here, the hand rehabilitation robot is required to help the volunteer's finger bend to a fixed angle. The DIP joint of the index finger is selected for this purpose. The following PID control method is used in the experiment for comparison

$$u(k) = K_p e(k) + K_i \sum_{j=0}^{k} e(j) + K_d(e(k) - e(k-1)),$$

where $e(k)$ denotes the error between the actual finger's bending angle and the desired finger's bending angle; K_p, K_i and K_d are the proportional gain, the integral gain and the derivative gain.

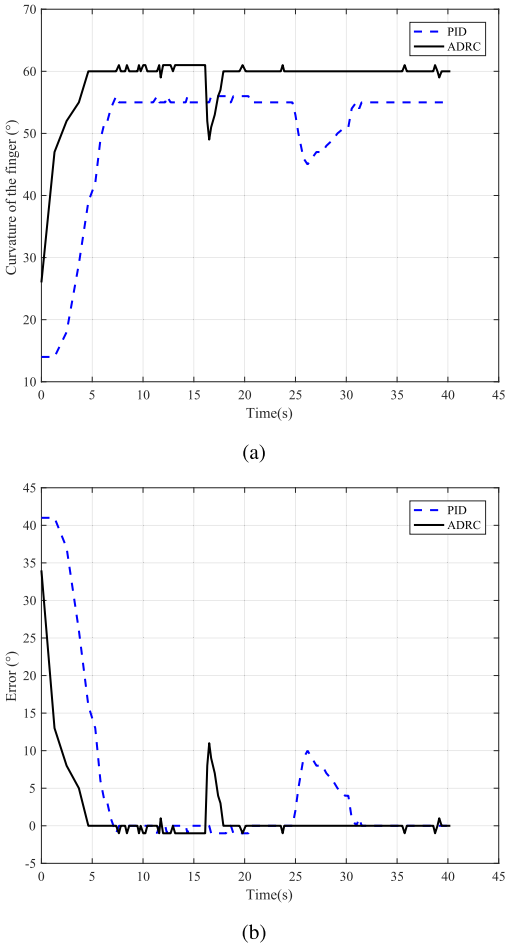

FIGURE 12. Performance of controlling the finger's bending angle to a fixed position under the PID controller and the ADRC controller. (a) Profiles of the finger's bending angle control under the PID controller and the ADRC controller. (b) Control errors of the PID controller and the ADRC controller.

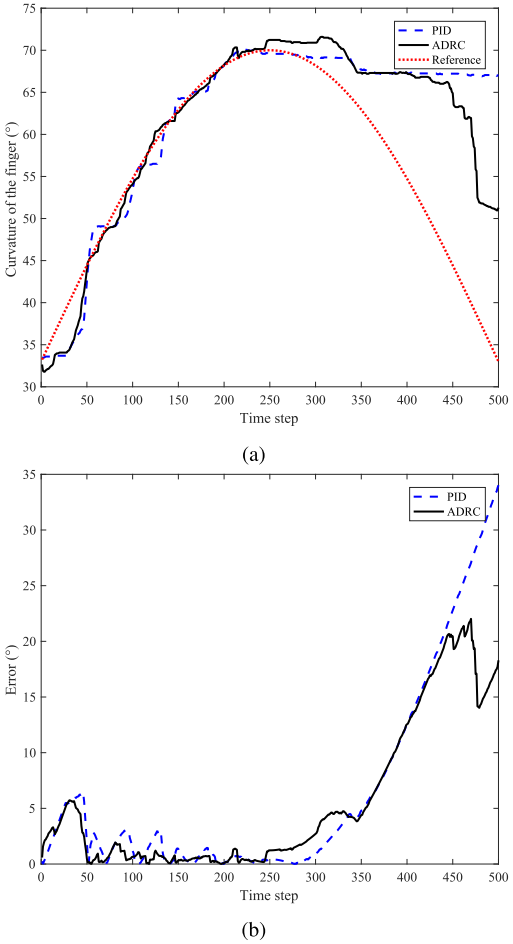

FIGURE 13. Performance of controlling the finger's bending angle to tracking a sinusoidal trajectory under the PID controller and the ADRC controller. (a) Profiles of the finger's bending angle control under the PID controller and the ADRC controller. (b) Control errors of the PID controller and the ADRC controller.

The control objective for the ADRC controller is $\theta_d(k) = 60°$ and the control objective of the PID controller is $\theta_d(k) = 55°$. Set $k_p = 1500$, $b = 1.1$ and $w = 0.001$ in the ADRC algorithm. The parameters for the PID controller are $K_p = 1500$, $K_i = 0.01$ and $K_d = 0$. These parameters are selected by the "trail and error" method to ensure the good control performance of the PID controller and the ADRC controller. In addition, to test the ability of disturbance rejection, an external disturbance is added to the robot system after the finger's angle has reached the desired position. The experimental results are shown in Fig. 12.

It can be seen from Fig. 12 that both the ADRC and the PID are able to overcome the disturbance influence. It takes about 2ms for the ADRC to overcome the influence caused by the disturbance, while the time used by the PID is about 7ms. Therefore, the ADRC controller has a faster response than the PID controller, which demonstrates a better disturbance rejection ability of the ADRC controller.

Next, the DIP joint of the index finger is required to track a sinusoidal signal which is set as follows

$$\theta_d(k) = 32 \sin(\pi k/500) + 33,$$

where $k \in \{0, 1, \cdots, 500\}$.

In the experiment, the parameters of the ADRC controller are set as $k_p = 3800$, $b = 7.5$ and $w = 0.005$; and the parameters for the PID controller are $K_p = 1000$, $K_i = 1$ and $K_d = 52$. The experimental results are shown in Fig. 13. It can be seen that the profile of the finger's bending angle based on the ADRC controller is smoother than the one based on the PID controller.

2) COMPARATIVE STUDY OF "ILC + ADRC" AND ILC

In the previous study [39], it has been shown that using the ILC algorithm can achieve a satisfactory control performance. In order to verify the improvement of the proposed "ILC + ADRC" controller, the following comparative experiment has been made. In this experiment, the index finger's

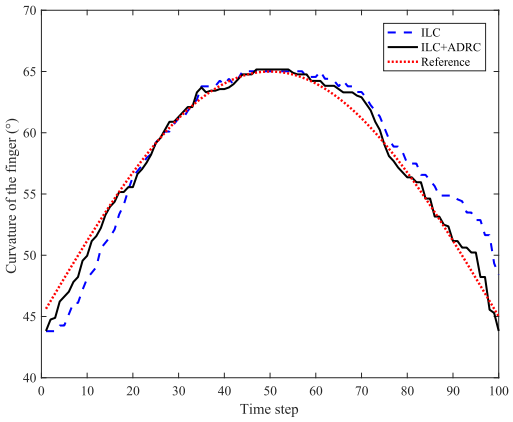

(a)

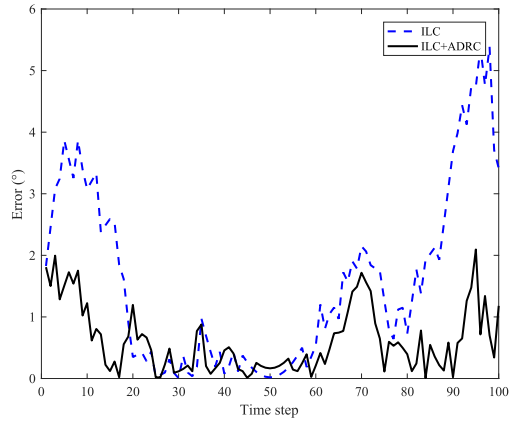

(b)

FIGURE 14. Performance of controlling the finger's bending angle to tracking a sinusoidal trajectory under the ILC controller and the "ILC + ADRC" controller. (a) Sinusoidal signal tracking profiles under the ILC controller and the "ILC + ADRC" controller. (b) Trajectory tracking errors under the ILC controller and the "ILC + ADRC" controller.

DIP joint is required to track the following sinusoidal signal

$$\theta_d(k) = 20\sin(\pi k/100) + 45, \tag{12}$$

where $k \in \{0, 1, \cdots, 100\}$.

It has been found that the best performance ILC controller u_{ILC} can be obtained under the gains of $k_{p1} = 800$ and $k_{p2} = 200$. If u_{ILC} is used to control the finger exoskeleton without any feedback control, the control performance is shown in Fig. 14 (see the blue dash line). Then this u_{ILC} is combined with the ADRC algorithm with parameters $k_p = 1000$, $b = 15$ and $w = 12$. The control performance of this composite controller is also shown in Fig. 14 (see the green solid line). The result shows that the tracking error of the proposed "ILC + ADRC" algorithm is less than 2°, while the tracking error of the ILC algorithm can reach 5°, which illustrates that the proposed "ILC +ADRC" controller can achieve a better performance than the previous study [39].

TABLE 1. Comparison of the R-square of four controllers.

parameters	PID	ADRC	ILC	ILC + ADRC
K_p	1000	-	-	-
K_i	1	-	-	-
K_d	52	-	-	-
k_p	-	3800	-	1000
b	-	7.5	-	15
w	-	0.005	-	12
p_1	-	-	800	800
p_2	-	-	200	200
R-square	0.036	0.43	0.805	0.983

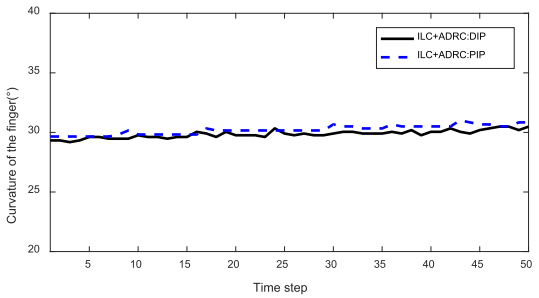

(a)

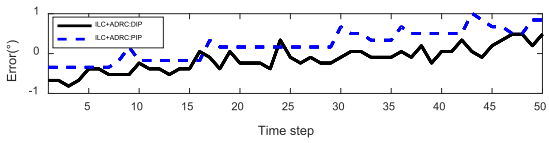

(b)

FIGURE 15. Performance of simultaneously controlling the finger's DIP and PIP joints to 30° under the proposed "ILC + ADRC" controller. (a) Profiles of the PIP joint and DIP joint under the proposed "ILC + ADRC" controller. (b) Profiles of the control error of the PIP joint and DIP joint under the proposed "ILC + ADRC" controller.

3) COMPARATIVE STUDY OF "ILC + ADRC", ADRC, ILC AND PID

This section gives a comparative table which shows the comparisons between four candidate controllers: "ILC + ADRC", ADRC, ILC and PID. One criterion is used to evaluate the control performance: the coefficient of multiple determination, R-square, which is defined as follows

$$R\text{-}square = 1 - \frac{\sum_{k=1}^{N}(\theta_d(k) - \theta(k))^2}{\sum_{k=1}^{N}(\theta_d(k) - \bar{\theta}_d)^2},$$

where $\bar{\theta}_d = \sum_{k=1}^{N}\theta_d(k)$. If R-square is close to 1, it indicates that the tracking error is small.

The result is shown in Table 1, which reveals the sequence of the control performance is: the proposed "ILC + ADRC" controller better than the "ILC" controller better than the "ADRC" controller and better than the "PID" controller.

4) SIMULTANEOUS CONTROL OF PIP AND DIP JOINTS

This section further verifies the performance of the proposed "ILC + ADRC" control algorithm by considering the simultaneous control of DIP joint and PIP joint. Here, both the DIP joint and the PIP joint are required to reach the position of 30°. The parameters of the proposed controller are set that: $k_p = 700$, $b = 0.5$, $w = 0.6$ for the DIP joint; $k_p = 700$, $b = 0.5$, $w = 1.2$ for the PIP joint. Experimental results are shown in Fig. 15 where the root mean square control error and the maximum control error of the DIP joint are 0.35° and 0.82°, respectively; and the root mean square control error and the maximum control error of the PIP joint are 0.43° and 1.01°, respectively. These results have illustrated that the proposed controller can simultaneously control the PIP and DIP joints well.

VI. CONCLUSION AND FUTURE WORK

This paper proposes a wearable hand rehabilitation robot for the finger's flexion and extension. This robot adopts the cable-driven approach for the long-distance power transmission and the entire control system is placed in the backpack. This setup can reduce the extra weight applied on the patient's hand and arm, which is better for the function recovery of the upper limb. The design of the hand exoskeleton has a modularized structure. Each finger exoskeleton is composed of several standard "shells" and "connecting rods" components, which can be easily replaced and repaired. Therefore, this modularized structure can provide conveniences for the robot's assembly, removal, repair and update. Some physical and software limits are added in the hand rehabilitation robot for ensuring the patient's safety. In addition, the workspace analysis of the robot shows that the finger's movement range is not constrained by the proposed robot. For the control system, a curvature sensor is added to measure the finger's bending angle. Then, an "ILC + ADRC" controller is proposed to control the robot for achieving the finger's flexion and extension. This controller is featured by the disturbance rejection ability of the ADRC controller and the ILC controller's ability of dealing with the repetitive training manner. Experiments have verified the function of the proposed hand rehabilitation robot and the effectiveness of the proposed "ILC + ADRC" controller.

In the future, some improvements are to be made on the proposed hand exoskeleton prototype from both the mechanical design and the control. For example, some passive degrees of freedom can be employed in the mechanical design to further improve the rotation axes alignment between the user's finger and the exoskeleton (see an interesting design example in [40]). Further optimization of the robot's design is to be conducted based on the patient's feedbacks. In addition, the proposed controller can only achieve the finger's position control. To increase the compliance between the patient and the robot, advanced force control algorithms, such as the impedance control and the admittance control, are to be studied. It is also noted that this paper only provides a proof of concept of the proposed hand rehabilitation robot. Clinical tests are to be made in the future work.

REFERENCES

[1] S. Mazzoleni, L. Puzzolante, L. Zollo, P. Dario, and F. Posteraro, "Mechanisms of motor recovery in chronic and subacute stroke patients following a robot-aided training," *IEEE Trans. Haptics*, vol. 7, no. 2, pp. 175–180, Apr./Jun. 2014.

[2] D. Zanotto, P. Stegall, and S. K. Agrawal, "Adaptive assist-as-needed controller to improve gait symmetry in robot-assisted gait training," in *Proc. IEEE Int. Conf. Robot. Autom.*, Hong Kong, May 2014, pp. 724–729.

[3] J.-C. Metzger, O. Lambercy, A. Califfi, F. M. Conti, and R. Gassert, "Neurocognitive robot-assisted therapy of hand function," *IEEE Trans. Haptics*, vol. 7, no. 2, pp. 140–149, Apr./Jun. 2014.

[4] S. R. Soekadar *et al.*, "Hybrid EEG/EOG-based brain/neural hand exoskeleton restores fully independent daily living activities after quadriplegia," *Sci. Robot.*, vol. 1, no. 1, p. eaag3296, 2016.

[5] P. Langhorne, F. Coupar, and A. Pollock, "Motor recovery after stroke: A systematic review," *Lancet Neurol.*, vol. 8, no. 8, pp. 741–754, Aug. 2009.

[6] C. D. Takahashi *et al.*, "Robot-based hand motor therapy after stroke," *Brain*, vol. 131, pp. 425–437, Feb. 2008.

[7] A. C. McConnell *et al.*, "Robotic devices and brain-machine interfaces for hand rehabilitation post-stroke," *J. Rehabil. Med.*, vol. 49, no. 6, pp. 449–460, 2017.

[8] Z. Yue, X. Zhang, and J. Wang, "Hand rehabilitation robotics on poststroke motor recovery," *Behav. Neurol.*, vol. 2017, Nov. 2017, Art. no. 3908135.

[9] J. Chen, D. Nichols, E. B. Brokaw, and P. S. Lum, "Home-based therapy after stroke using the hand spring operated movement enhancer (HandSOME)," *IEEE Trans. Neural Syst. Rehabil. Eng.*, vol. 25, no. 12, pp. 2305–2312, Dec. 2017.

[10] C. N. Schabowsky, S. B. Godfrey, R. J. Holley, and P. S. Lum, "Development and pilot testing of HEXORR: Hand EXOskeleton rehabilitation robot," *J. NeuroEng. Rehabil.*, vol. 7, p. 36, Jul. 2010.

[11] M. Cempini, M. Cortese, and N. Vitiello, "A powered finger–thumb wearable hand exoskeleton with self-aligning joint axes," *IEEE/ASME Trans. Mechatronics*, vol. 20, no. 2, pp. 705–716, Apr. 2015.

[12] S. W. Lee, K. A. Landers, and H.-S. Park, "Development of a biomimetic hand exotendon device (BiomHED) for restoration of functional hand movement post-stroke," *IEEE Trans. Neural Syst. Rehabil. Eng.*, vol. 22, no. 4, pp. 886–898, Jul. 2014.

[13] C. J. Nycz, T. Bützer, O. Lambercy, J. Arata, G. S. Fischer, and R. Gassert, "Design and characterization of a lightweight and fully portable remote actuation system for use with a hand exoskeleton," *IEEE Robot. Autom. Lett.*, vol. 1, no. 2, pp. 976–983, Jul. 2016.

[14] G. G. Fluet, A. S. Merians, Q. Qiu, A. Davidow, and S. V. Adamovich, "Comparing integrated training of the hand and arm with isolated training of the same effectors in persons with stroke using haptically rendered virtual environments, a randomized clinical trial," *J. Neuroeng. Rehabil.*, vol. 11, Aug. 2014, Art. no. 126.

[15] H. C. Fischer *et al.*, "Use of a portable assistive glove to facilitate rehabilitation in stroke survivors with severe hand impairment," *IEEE Trans. Neural Syst. Rehabil. Eng.*, vol. 24, no. 3, pp. 344–351, Mar. 2016.

[16] R. F. Beer, M. D. Ellis, B. G. Holubar, and J. P. A. Dewald, "Impact of gravity loading on post-stroke reaching and its relationship to weakness," *Muscle Nerve*, vol. 36, no. 2, pp. 242–250, 2007.

[17] S.-S. Yun, B. B. Kang, and K.-J. Cho, "Exo-glove PM: An easily customizable modularized pneumatic assistive glove," *IEEE Robot. Autom. Lett.*, vol. 2, no. 3, pp. 1725–1732, Jul. 2017.

[18] P. Polygerinos, Z. Wang, K. C. Galloway, R. J. Wood, and C. J. Walsh, "Soft robotic glove for combined assistance and at-home rehabilitation," *Robot. Auto. Syst.*, vol. 73, pp. 135–143, Nov. 2015.

[19] L. Connelly, Y. Jia, M. L. Toro, M. E. Stoykov, R. V. Kenyon, and D. G. Kamper, "A pneumatic glove and immersive virtual reality environment for hand rehabilitative training after stroke," *IEEE Trans. Neural Syst. Rehabil. Eng.*, vol. 18, no. 5, pp. 551–559, Oct. 2010.

[20] H. K. Yap, N. Kamaldin, J. H. Lim, F. A. Nasrallah, J. C. H. Goh, and C.-H. Yeow, "A magnetic resonance compatible soft wearable robotic glove for hand rehabilitation and brain imaging," *IEEE Trans. Neural Syst. Rehabil. Eng.*, vol. 25, no. 6, pp. 782–793, Jun. 2017.

[21] Z. Tang, S. Sugano, and H. Iwata, "A finger exoskeleton for rehabilitation and brain image study," in *Proc. IEEE Int. Conf. Intell. Robots Syst.*, Seattle, WA, USA, Jun. 2013, pp. 1–6.

[22] J. Iqbal, N. G. Tsagarakis, and D. G. Caldwell, "Human hand compatible underactuated exoskeleton robotic system," *Electron. Lett.*, vol. 50, no. 7, pp. 494–496, Mar. 2014.
[23] J. Iqbal, N. G. Tsagarakis, and D. G. Caldwell, "Four-fingered lightweight exoskeleton robotic device accommodating different hand sizes," *Electron. Lett.*, vol. 51, no. 12, pp. 888–890, Jun. 2015.
[24] T. T. Worsnopp, M. A. Peshkin, J. E. Colgate, and D. G. Kamper, "An actuated finger exoskeleton for hand rehabilitation following stroke," in *Proc. IEEE Int. Conf. Rehabil. Robot.*, Noordwijk, The Netherlands, Jun. 2007, pp. 896–901.
[25] A. Chiri, N. Vitiello, F. Giovacchini, S. Roccella, F. Vecchi, and M. C. Carrozza, "Mechatronic design and characterization of the index finger module of a hand exoskeleton for post-stroke rehabilitation," *IEEE/ASME Trans. Mechatronics*, vol. 17, no. 5, pp. 884–894, Oct. 2012.
[26] M. A. Delph, S. A. Fischer, P. W. Gauthier, C. H. M. Luna, E. A. Clancy, and G. S. Fischer, "A soft robotic exomusculature glove with integrated sEMG sensing for hand rehabilitation," in *Proc. IEEE Int. Conf. Rehabil. Robot.*, Seattle, WA, USA, Jun. 2013, pp. 1–7.
[27] H. In, B. B. Kang, M. Sin, and K. J. Cho, "Exo-glove: A wearable robot for the hand with a soft tendon routing system," *IEEE Robot. Autom. Mag.*, vol. 22, no. 1, pp. 97–105, Mar. 2015.
[28] R. Colombo *et al.*, "Robotic techniques for upper limb evaluation and rehabilitation of stroke patients," *IEEE Trans. Neural Syst. Rehabil. Eng.*, vol. 13, no. 3, pp. 311–324, Sep. 2005.
[29] Y. Park, I. Jo, and J. Bae, "Development of a dual-cable hand exoskeleton system for virtual reality," in *Proc. IEEE/RSJ Int. Conf. Intell. Robots Syst.*, Daejeon, South Korea, Oct. 2016, pp. 1019–1024.
[30] J. Wu, J. Huang, Y. Wang, and K. Xing, "A wearable rehabilitation robotic hand driven by PM-TS actuators," in *Proc. 3rd Int. Conf. Intell. Robot. Appl.*, Shanghai, China, Nov. 2010, pp. 440–450.
[31] C. L. Jones, F. Wang, R. Morrison, N. Sarkar, and D. G. Kamper, "Design and development of the cable actuated finger exoskeleton for hand rehabilitation following stroke," *IEEE/ASME Trans. Mechatronics*, vol. 19, no. 1, pp. 131–140, Feb. 2014.
[32] W. Meng, S. Q. Xie, Q. Liu, C. Z. Lu, and Q. Ai, "Robust iterative feedback tuning control of a compliant rehabilitation robot for repetitive ankle training," *IEEE/ASME Trans. Mechatronics*, vol. 22, no. 1, pp. 173–184, Feb. 2017.
[33] N. Ajjanaromvat and M. Parnichkun, "Trajectory tracking using online learning LQR with adaptive learning control of a leg-exoskeleton for disorder gait rehabilitation," *Mechatronics*, vol. 51, pp. 85–96, May 2018.
[34] C. T. Freeman, "Upper limb electrical stimulation using input-output linearization and iterative learning control," *IEEE Trans. Control Syst. Technol.*, vol. 23, no. 4, pp. 1546–1554, Jul. 2015.
[35] X. Zhu and J. Wang, "Double iterative compensation learning control for active training of upper limb rehabilitation robot," *Int. J. Control Autom. Syst.*, vol. 16, no. 3, pp. 1312–1322, 2018.
[36] X. Li, Y.-H. Liu, and H. Yu, "Iterative learning impedance control for rehabilitation robots driven by series elastic actuators," *Automatica*, vol. 90, pp. 1–7, Apr. 2018.
[37] R. Zheng and J. Li, "Kinematics and workspace analysis of an exoskeleton for thumb and index finger rehabilitation," in *Proc. IEEE Int. Conf. Robot. Biomimetics*, Tianjin, China, Dec. 2010, pp. 80–84.
[38] R. Yang, M. Sun, and Z. Chen, "Active disturbance rejection control on first-order plant," *J. Syst. Eng. Electron.*, vol. 22, no. 1, pp. 95–102, Feb. 2011.
[39] S. Liu, D. Meng, L. Cheng, and M. Chen, "An iterative learning controller for a cable-driven hand rehabilitation robot," in *Proc. 43rd Annu. Conf. IEEE Ind. Electron. Soc.*, Beijing, China, Oct. 2017, pp. 5701–5706.
[40] X. Lu, Z. Yang, Y. Chen, and J. Wang, "Structure design of a wearable device for hand rehabilitation," in *Proc. 9th Int. Symp. Comput. Intell. Design*, Hangzhou, China, Dec. 2016, pp. 93–95.

LONG CHENG (M'09–SM'14) received the B.S. degree (Hons.) in control engineering from Nankai University, Tianjin, China, in 2004, and the Ph.D. degree (Hons.) in control theory and control engineering from the Institute of Automation, Chinese Academy of Sciences, Beijing, China, in 2009.

In 2010, he was a Post-Doctoral Research Fellow with the Department of Mechanical Engineering, University of Saskatchewan, Saskatoon, SK, Canada, for eight months, and he was with the Mechanical and Industrial Engineering Department, Northeastern University, Boston, MA, USA, from 2010 to 2011. From 2013 to 2014, he was a Visiting Scholar with the Electrical and Computer Engineering Department, University of California at Riverside, Riverside, CA, USA. He is currently a Professor with the Laboratory of Complex Systems and Intelligent Science, Institute of Automation, Chinese Academy of Sciences. He is also a Professor with University of Chinese Academy of Sciences. He has published over 100 technical papers in peer-refereed journals and prestigious conference proceedings. His research interests include intelligent control of smart materials, coordination of multiagent systems, neural networks, and their applications to robotics.

Dr. Cheng is an Associate Editor of the IEEE TRANSACTIONS ON CYBERNETICS. He is also an Editorial Board Member of *Neurocomputing* and the *International Journal of Systems Science*.

MIAO CHEN received the B.S. degree in automation from Beijing Information Science and Technology University, Beijing, China, in 2015, and the M.S. in control engineering from the Institute of Automation, Chinese Academy of Sciences, Beijing, in 2018. He is currently an Artificial Intelligence R&D Engineer at China Mobile. His research interests are mainly in intelligent robot systems and artificial intelligence.

ZHENGWEI LI received the B.S. degree in vehicle engineering from the Shandong University of Technology, Zibo, China, in 2016. He is currently pursuing the master's degree with the Institute of Automation, Chinese Academy of Sciences, Beijing, China. His research interests is the sensor technology and soft robotics.